Experimental study of interaction of microwaves with a nonmagnetized pulsed-plasma column

A. Singh, W. W. Destler, P. Catravas,[a] and J. Rodgers
Laboratory for Plasma Research, University of Maryland, College Park, Maryland 20742

The time evolution of backscattered and sidescattered microwaves from a plane conductor covered by a pulsed-plasma column has been studied; transmitted signals along the axial and transverse directions of the column have also been studied. The incident microwaves are at a cw power level varying from a few milliwatts to a few watts. The cw nature of the signal makes it possible to observe the fine structure in the time evolution of the interactions. The plasma is generated by an array of plasma guns embedded in the conducting plate. The plasma density has a gradient in the axial direction and contains regions of subcritical and supercritical plasma density. Reductions in the backscattered radiation down to the lowest measurable levels with available equipment are observed for durations that are an order of magnitude longer than the duration of the current pulse that generated the plasma. Variations caused by changes in the charging potential on the plasma gun capacitor bank, the pressure of the background gas, and the frequency and power level of the incident microwaves are reported. The attenuation in the backscattered radiation decreases with increasing pressure, especially at lower charging potentials. There is a close correlation between the timing and location of sidescattered signals and the transition of the critical density layer across the axial position of the detectors for the scattered signal. The amplitude of the scattered signal was also measured. Estimates have been made for the percentage of incident power accounted for by scattering. Models are discussed for absorption of microwaves in the plasma.

I. INTRODUCTION

Compared to conventional absorbers of microwaves, plasmas offer the possibility of a wider frequency coverage, switchability, and tunability. The reduction in microwave backscatter and effective absorption of microwaves by plasmas have thus been the subject of investigation at a number of laboratories.[1-8] The nature of the plasmas studied has included isotropic and magnetized plasmas, those generated by photoionization or by arc discharge, those that are collisional or collisionless, and those that are confined in waveguides, cones, or enclosures. We have reported previous studies at this laboratory dealing with experiments using pulsed microwaves of 30 ns duration at megawatt power levels.[9] Attenuation of the order of 30 dB in the backscattered microwave signal from a conducting plate was achieved by generating a pulsed plasma in front of the plate using plasma guns embedded in the plate. Various phases of the time evolution of the interaction process were studied by varying the time lag between the triggering of the plasma and the firing of the source of microwaves (a large-orbit gyrotron). The background pressure was of the order of 0.1 mTorr. At such a pressure electron-neutral collisions were not considered to be a major cause of the observed attenuation. Different parametric instabilities were considered as possible causes, and threshold values were estimated. Consequently, in spite of the high microwave power level, only the oscillating two stream instability appeared to have a sufficiently high growth rate to significantly affect the wave amplitude. The possibility of enhanced absorption due to a transverse structure at the critical density layer was also noted.

The present study was motivated by a desire to understand more clearly the nature of the underlying phenomenon, and thus to be able to optimize its application. To this end, the experiment was modified so as to use continuous-wave microwaves in the power range of a few milliwatts to a few watts. Consequently, the fine structure in the sequence of development of the microwave-plasma interaction can be studied systematically. The resultant digitally stored data can be analyzed to give a time resolution down to nanosecond range. In addition, the lower-power microwave sources allow a much larger number of experiments in a given span of time and thereby permit a much more complete exploration of the parameter space. Finally, the low-power experiments allow for an investigation of the rf-plasma interactions at power densities seven orders of magnitude lower than the previous studies, thereby shedding additional light on the presence of any nonlinear effects. The operating parameters that were varied included the charging potential on the capacitor bank that fed the plasma guns, the pressure of the background gas, and the frequency and power level of the incident microwaves.

In Sec. II of this paper the experimental setup and techniques used are described. The dependence of backscattered and axially transmitted microwave signals on operating parameters is presented in Secs. III and IV, respectively. Results on the time evolution of both sidescattered and transverse transmission signals are given in Secs. V and VI, respectively, and their correlation is presented in Sec. VII. Observations on the amplitude of the sidescat-

[a]Present address: Department of Electrical Engineering, Massachusetts Institute of Technology, Cambridge, MA.

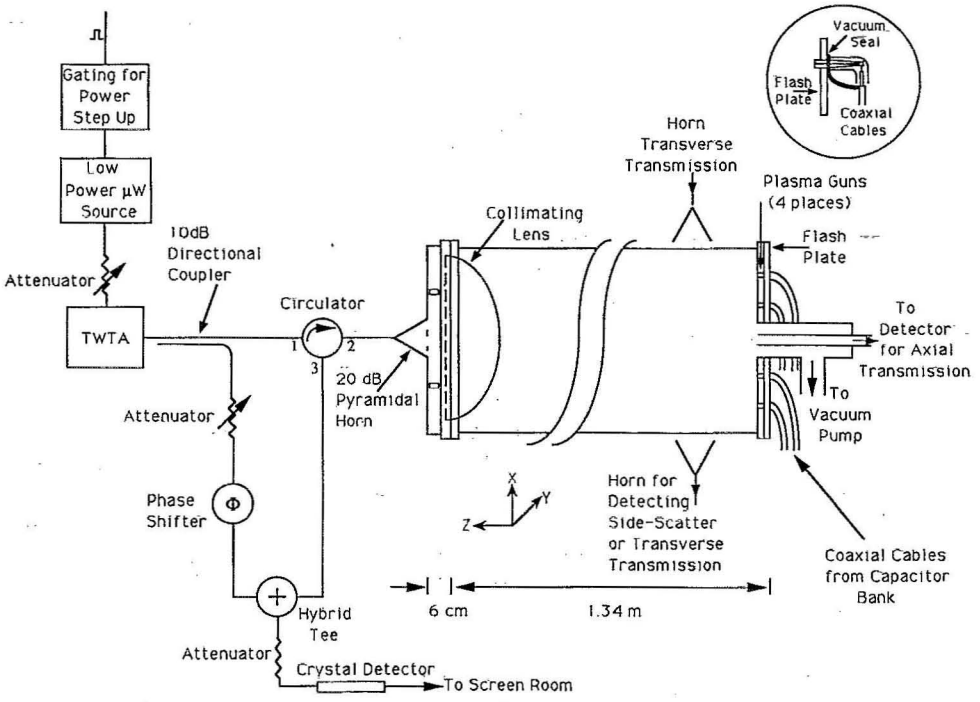

FIG. 1. Schematic diagram of the experimental setup.

tered signal and estimation of its power as a percentage of the incident signal are given in Secs. VIII and IX, respectively. Results of simulations of reduction in backscattered signal in a transversely homogeneous plasma are presented in Sec. X, the effects of the process of generation of the plasma on its lack of homogeneity are discussed in Sec. XI, and a model based on resonance absorption in a transversely inhomogeneous plasma is outlined in Sec. XII. Conclusions are summarized in Sec. XIII.

II. THE EXPERIMENTAL SETUP AND TECHNIQUES USED

A schematic diagram of the setup is shown in Fig. 1. The microwave-plasma interaction occurred in an acrylic tube 1.35 m long with a diameter of 30 cm. The plasma was generated by an array of four plasma guns embedded in a stainless-steel plate attached to one end of the tube. Each gun consisted of a spark plug with the space between inner and outer conductors filled with an epoxy containing titanium hydride. These guns produced what was essentially a hydrogen plasma when an arc discharge current was passed through them.

The other side of the tube was closed by a plexiglas plate, or a microwave lens for measurements at 10 GHz. The incident microwaves were launched by a standard-gain horn having a gain of 20 dB. Its distance from the lens was adjusted to minimize changes in the backscattered signal when a shorting plate was moved axially back and forth on the other end of the acrylic tube. A minimum of 1.5:1 in the ratio of highest to lowest values of backscattered signals was obtained for a frequency of 10 GHz when the distance between the mouth of the horn and the front (flat) face of the lens was 6 cm. This procedure was adopted so as to obtain as good an approximation as possible of a plane-wave front emerging from the curved rear surface of the lens.

The incident microwaves were generated by two low-power (0–100 mW) sources at 10 and 13.77 GHz. Where higher power was required, a travelling-wave tube amplifier was added. Power to the 20 dB horn was fed via a circulator having a nominal directivity of 30 dB. This separated the outgoing signal from the reflected signal. The latter was detected and fed by coaxial cable to a digital oscilloscope. Using this kind of transmit-receive arrangement employing a single horn, measurements of the attenuation in the backscattered signal could be made with a dynamic range of up to about 30 dB (a figure limited by the directivity of the directional coupler).

To study the extent of delay between initiation of discharge current and the reduction in backscattered signal, the two were probed simultaneously as shown in Fig. 2. It

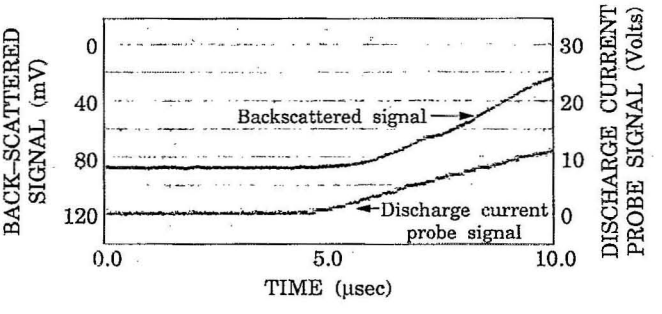

FIG. 2. Time relationship between start of plasma discharge current and the start of reduction in backscattered signal (the latter increases downward in the graph). Delay is of the order of 1 μs.

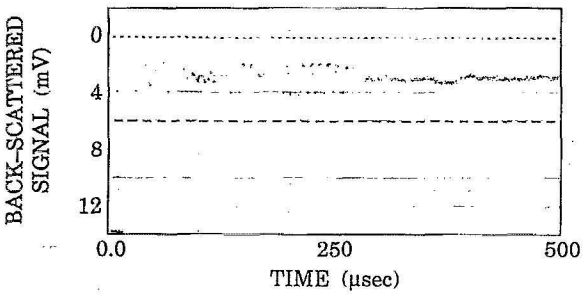

FIG. 3. Early phase of backscattered signal (without balancing out of parasitic reflection); frequency is 10 Ghz, charging potential is 8.5 kV, and pressure $\simeq$100 mTorr.

is seen that the delay is of the order of 1 μs. Furthermore, in this initial phase the two traces do not indicate a highly nonlinear relationship between the backscattered signal and the discharge current (notice that in the graph, the backscattered signal increases downwards).

The reflected signal has three main components: (a) the signal propagating through the plasma to the flash plate and back; (b) the signal reflected from the front surface of the plastic plate or the lens; and (c) the signal reflected from the plasma gradient itself. These three components together produce the detected signal, which has a cyclically varying nature and which contains information on the amplitudes as well as the relative phases of both the rf signals. In the first 200 μs or so, the fluctuations in the detected signal often showed segments of different periodicity, with a phase reversal in between. An example of such a trace is shown in Fig. 3. A possible explanation is that the backscattered signal is slightly shifted in frequency. This can be attributed to a Doppler shift by reflection from a layer whose location travels across the tube due to changes in the density profile.

Shifts in frequency can also result from rises and falls in density of the plasma with time.[10] The relatively slow fluctuations in the backscattered signal toward the end of the interaction period can be attributed to the effect of plasma density slowly decaying below critical value. This changes the effective dielectric constant of the plasma and produces a phase shift between reflections from the front and the rear ends of the tube.

The fluctuations in the detected backscattered rf signal are indicative of interference fringes resulting from its beating with parasitic reflections. While observations of interference fringes do provide useful information, they can also prevent accurate measurements of the amplitude of the backscattered signal. With this in view, a bridge circuit using a hybrid tee was included in the detector system as shown in Fig. 1. A signal tapped from the incident wave was used to cancel parasitic reflections such as from the surface of the lens. The amplitude and phase of the cancelling signal were adjusted to minimize the composite detected signal when the metal end plate was substituted temporarily by an anechoic box. Figure 4 shows the backscattered signal (a) without and (b) with the balancing out of parasitic reflections, in a typical case. It is seen that the fringes are considerably reduced, though not completely eliminated.

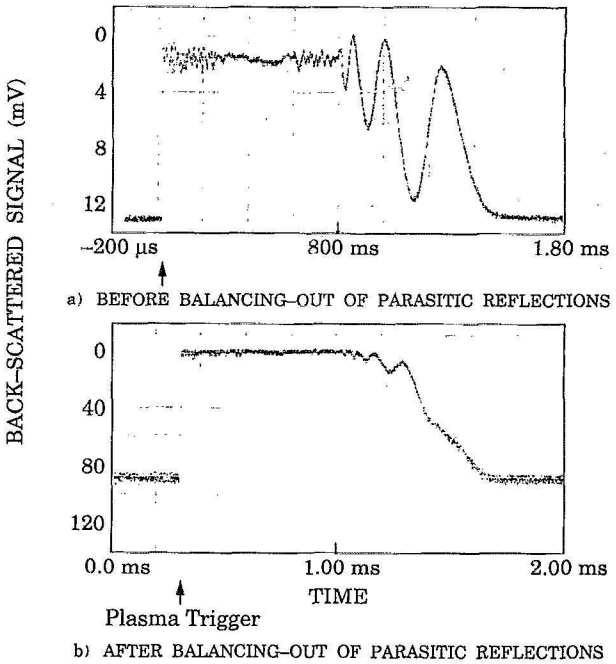

FIG. 4. Backscattered microwave signals (a) before and (b) after balancing out parasitic reflections from the lens and other surfaces. Frequency is 10 GHz, charging potential is 8.5 kV, and pressure is 100 mTorr.

In the case shown in Fig. 4(b), and other similar cases where the attenuation in backscattered signal is the highest, the trace becomes almost indistinguishable from the zero line. In order to increase the dynamic range of the measurement, a gating circuit was added to the amplitude modulation facility provided in the low-power oscillator. The timing of the gate was set in such a way that the power would be stepped up by a known factor in a time period when the attenuation due to the plasma was high. Thus, the detector could measure both the large backscattered signal without the plasma but with low incident power and also the attenuated backscattered signal at a higher incident power level without saturating the detector. Figures 5(a) and 5(b) show the detected traces without and with the gated upshift in power level of incident microwaves. In this way attenuation of the order of 30 dB could be measured. In our configuration where the same horn acts as the sending and the receiving horn, the accuracy was restricted by the limitation in directivity of the circulator employed as well as the microfluctuations in the plasma itself. These fluctuations also show up in the enhanced level of backscattered signal when the power is stepped up during the selected time gate, as seen in Fig. 5(b).

Observations on the axial transmission through the plasma column were also conducted. In this case an open-ended waveguide was used to sample the received signal at the surface of the flash plate.

For observations on sidescattered and transversely

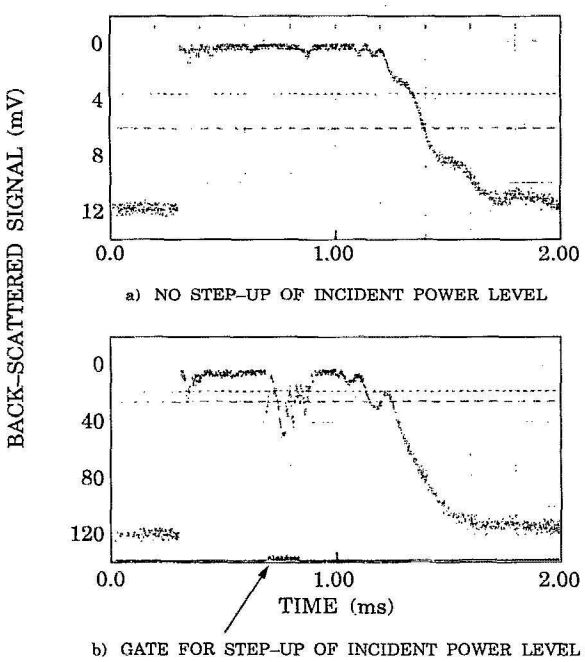

FIG. 5. Increase in dynamic range of measurement of attenuation by gated stepup of incident power level; frequency is 10 GHz, charging potential is 8.5 kV, and pressure is 100 mTorr.

transmitted radiation, auxiliary horns were used that were oriented radially, as shown in Fig. 1. Their locations and orientation are discussed in greater detail in Sec. V.

III. DEPENDENCE OF BACKSCATTERED SIGNAL ON OPERATING PARAMETERS

Using the setup described in the previous section, a series of experiments was conducted on the time evolution of the backscattered microwave signal as a function of various parameters. Typical results are summarized below.

Figure 6 shows the time evolution of the backscattered signal for different values of background pressure ranging from 15 mTorr to 10 Torr, when the charging potential was 8.5 kV. It is noticed that the duration of maximum attenuation is of the order of 600–800 μm. (The duration of the discharge current that generates the plasma is approximately 40 μm.) In general the duration is an order of magnitude higher than the duration observed in our high microwave power experiment.[9] In the present experiments there is a lens or a partition at the end of the tube opposite to the flash plate. This and the pressure of background gas are possible parameters helping to retain higher plasma densities for a longer time than in the previous studies where there was a direct connection to a large-orbit gyrotron at low background pressure with no interface in between.

Figure 7 shows the time evolution of the backscattered signal for plasma gun capacitor bank charging potentials of 8.5, 6.0, and 3.5 kV. The duration of the maximum attenuation decreases with reductions in the charging potential. It is seen that for 3.5 kV charging potential, the trace shows a decrease in attenuation followed by another in-

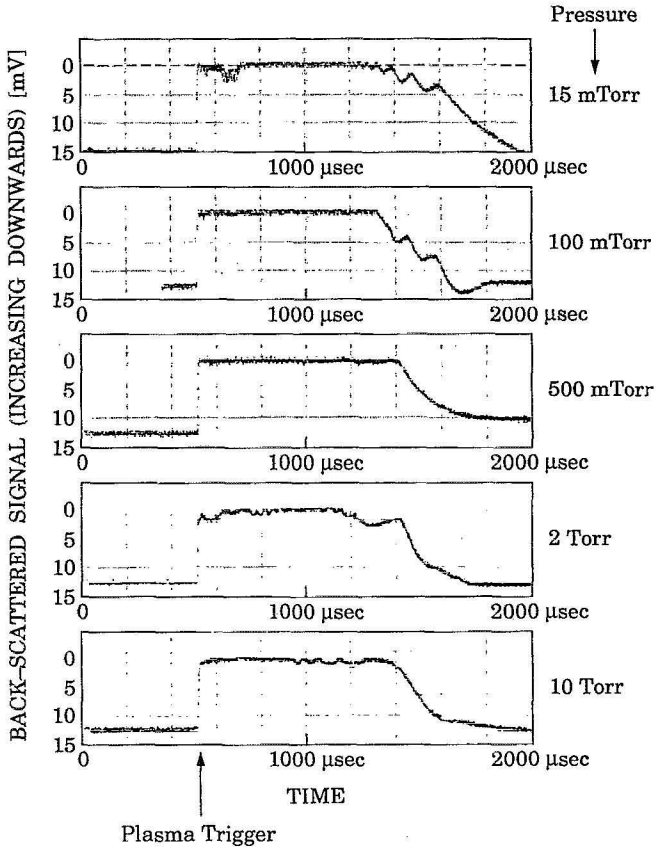

FIG. 6. Time evolution of backscattered signal at different values of background pressure; frequency is 10 GHz, and charging potential is 8.5 kV.

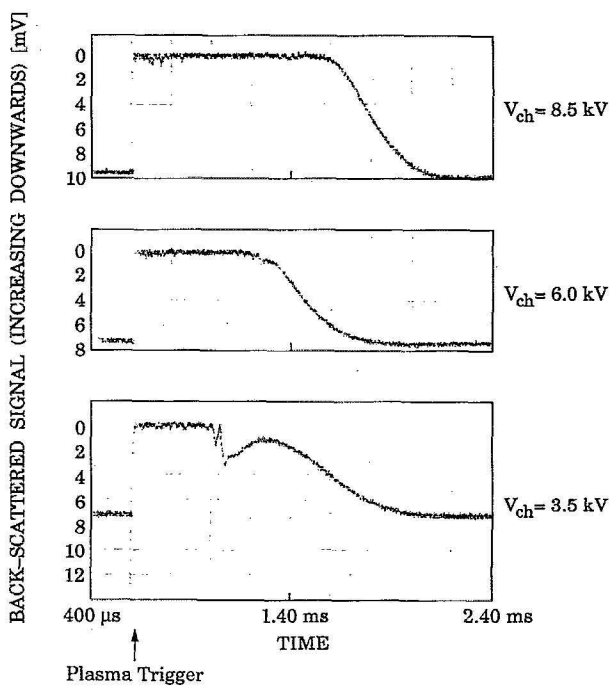

FIG. 7. Backscattered signal level as a function of time, at different values of charging potential V_{ch}; frequency is 10 GHz, pressure is 12 mTorr.

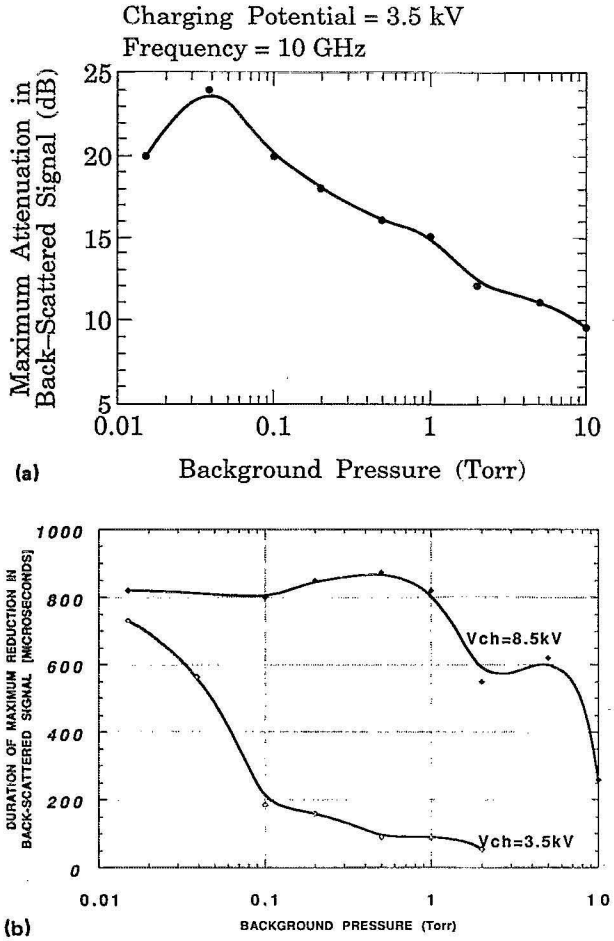

FIG. 8. (a) Variation of maximum attenuation in backscattered signal as a function of background pressure for a low value of charging potential (viz. 3.5 kV); frequency is 10 GHz. (b) Duration of maximum reduction in backscattered signal as a function of background pressure for charging potentials of 3.5 and 8.5 kV; frequency is 10 GHz.

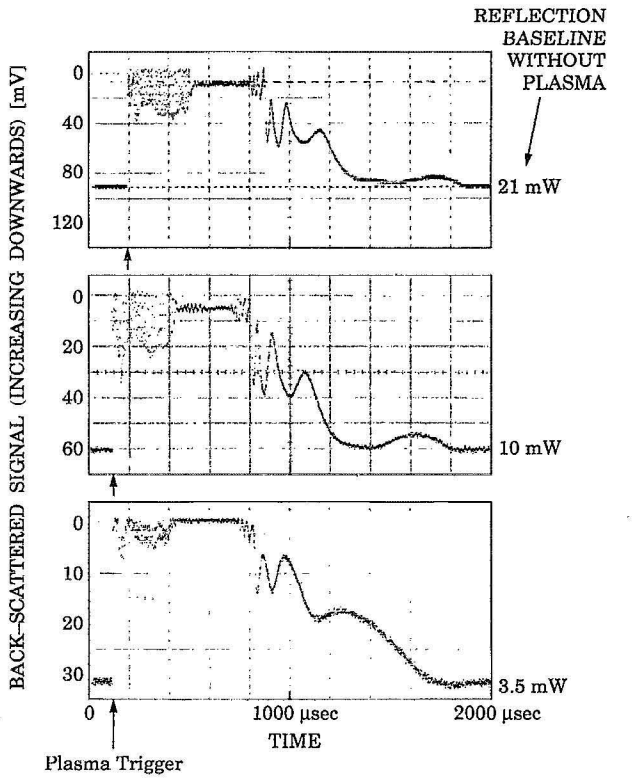

FIG. 9. Effect of variation of incident power level on time evolution of backscattered signal; frequency is 10 GHz, pressure is 24 mTorr.

crease. At higher charging potentials these two regimes appear to merge. It has also been observed that, when the charging potential is low, the maximum attenuation in each shot decreases with increase in pressure, as seen in Fig. 8(a) for the case of 3.5 kV. However, for 8.5 kV the variation of maximum attenuation with pressure could not be determined, because the detection system accuracy was limited in attenuation measurements to 30 dB or less. Figure 8(b) shows the duration of the maximum reduction in backscattered signal as a function of background pressure. It is seen that it falls noticeably for pressure above 0.1 Torr, for the case of 3.5 kV charging potential. However, for 8.5 kV charging potential it remains nearly constant up to 1 Torr and falls rapidly above 5 Torr.

The time evolution of the backscattered signal as a function of the incident microwave power level is shown in Fig. 9. The three traces represent a variation of 7:1 in the level of microwave power backscattered from the flash plate in the absence of the plasma. The sensitivity of the scale was adjusted to accommodate the received signal level. The bridge circuit was not fully balanced in this case, so that the traces do show the various phases of evolution of the plasma. The traces are not identical. However, over this power range the general nature of the behavior does not change significantly.

IV. DEPENDENCE OF AXIAL TRANSMISSION ON CHARGING POTENTIAL

In this set of experiments the microwave power level reaching the flash plate was sampled by an open-ended waveguide inserted into the flash plate on axis (as shown in Fig. 1). The time evolution of the received signal at charging potentials of 8.5, 6.0, and 3.5 kV is shown in Fig. 10. The period of high attenuation is followed by an increase in the signal, which in turn is followed by another period of increased attenuation. This effect is more prominent at the lowest charging potential of 3.5 kV. It is also reminiscent of a similar effect in the case of backscattered signal. The duration of the first period of high attenuation as a function of the charging potential is shown in Fig. 11. The variation is seen to be an almost linearly increasing function of charging potential. This can be attributed to the higher plasma density achieved with the larger charging potential, which then takes a longer time to deplete below the critical value at every location.

V. TIME EVOLUTION OF THE SIDESCATTERED SIGNAL

In studying the physical phenomena responsible for the reduction in the backscattered signal, it is also of importance to observe the nature of the sidescattered signal. This was done by detecting the signal picked up by a horn

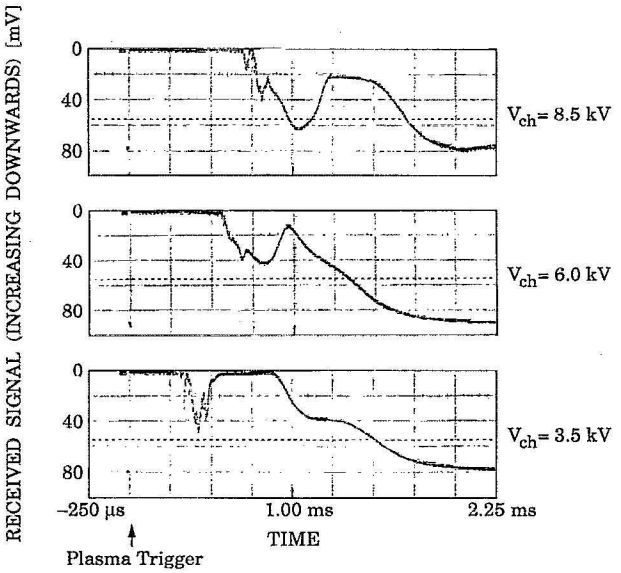

FIG. 10. Time evolution of axial transmission at different values of charging potential V_{ch}; frequency is 10 GHz, pressure is 15 mTorr. Microwaves turned on only briefly before plasma trigger.

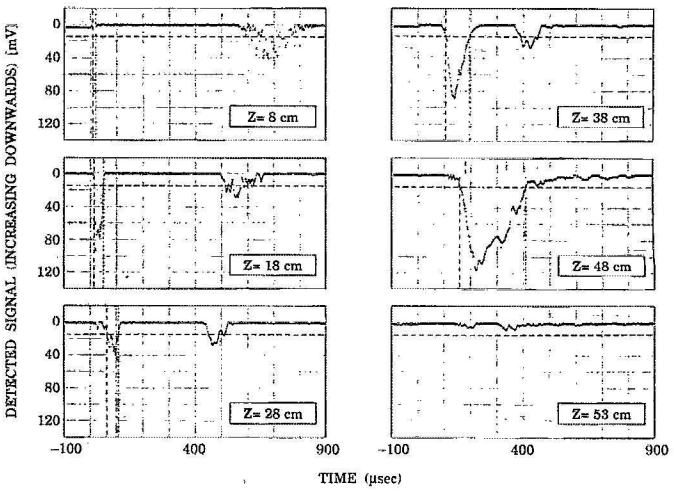

FIG. 12. Time evolution of sidescattered signal at various distances z from flash plate. Both sending and receiving horns have polarization of E field in the x direction (i.e., vertical). Frequency is 10 GHz, pressure is 15 mTorr, charging potential is 8.5 kV, and incident signal amplified by traveling-wave tube amplifier.

which pointed in the radial direction and which could be set at various distances from the flash plate in the axial direction (Fig. 1). Several orientations of the launching and receiving horns were studied. The orientation studied most extensively was one in which the E vectors of the two horns were aligned parallel to each other, which was referred to as the x direction. In another combination, the E vector of the receiving horn was oriented in the z direction. Finally, the launching horn was turned by 90° (its E vector now being in the y direction), which had the same effect as if the receiving horn and its supporting structure had been turned around in azimuth by 90°.

The sidescattered signal at various distances z from the flash plate is shown in Fig. 12 for the orientation of x and x for the horns. It is observed that the scattered signal consists of two groups of pulses. These are well separated in time at small values of z and tend to coalesce at larger values; they merge near $z=48$ cm. Beyond this distance the amplitude drops dramatically. As discussed in more detail later, the broad nature of this phenomenon is attributed to the fact that the sidescattering takes place mainly during those time periods when a layer of critical density transits across the given axial location of the receiving horn.

In a further study of possible nonlinear effects, the sidescattered power for the above orientations of horns was observed at a frequency of 13.774 GHz, while varying the incident power level over a range of 30 dB. Figure 13 shows the relationship of the two on a log-log scale. It is seen that the curve is nearly a straight line, with a slope of 1.046. These observations point to the fact that the incident and scattered power levels are linearly related over a 1000:1 power range.

Figures 14 and 15 show the sidescattered signal with its E vector in the z direction, for the cases where the sending horn had its E vector in the x and y directions, respectively. The feature of the two groups of pulses that

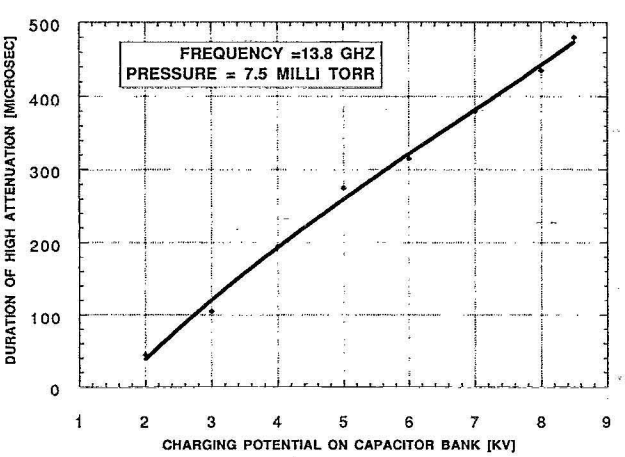

FIG. 11. Duration of period of high attenuation in axial transmission at different values of charging potential V_{ch}.

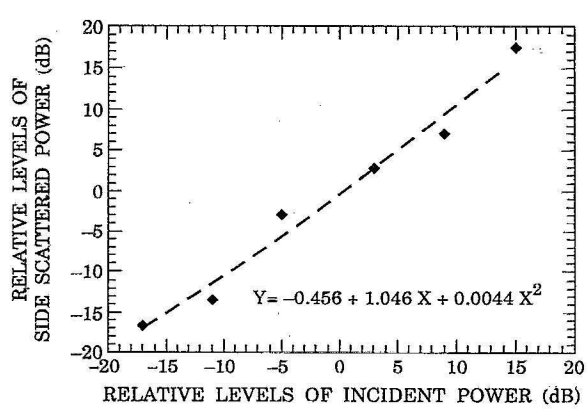

FIG. 13. Sidescattered power Y as a function of incident power level X.

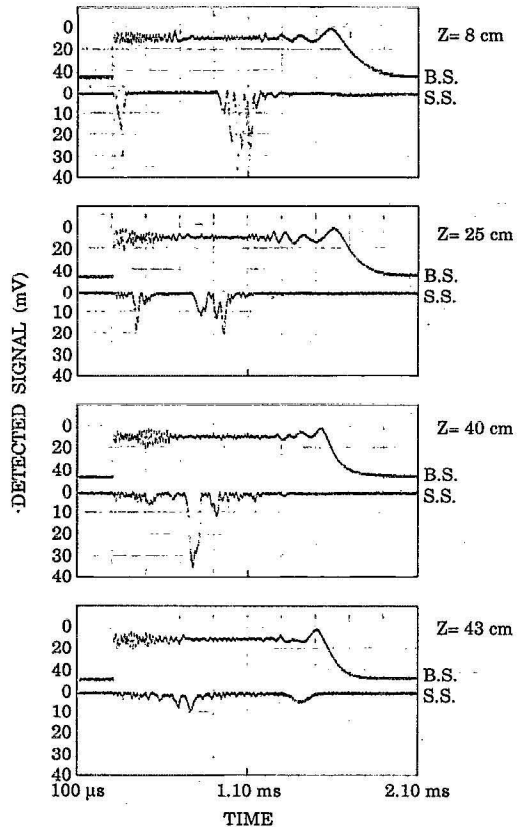

FIG. 14. Time evolution of backscattered signals (upper traces) and sidescattered signals (lower traces), at different distances z from flash plate; polarization of incident signal in x direction and that of scattered signal in z direction. Frequency is 10 GHz, charging potential is 8.5 kV, and pressure is 72 mTorr.

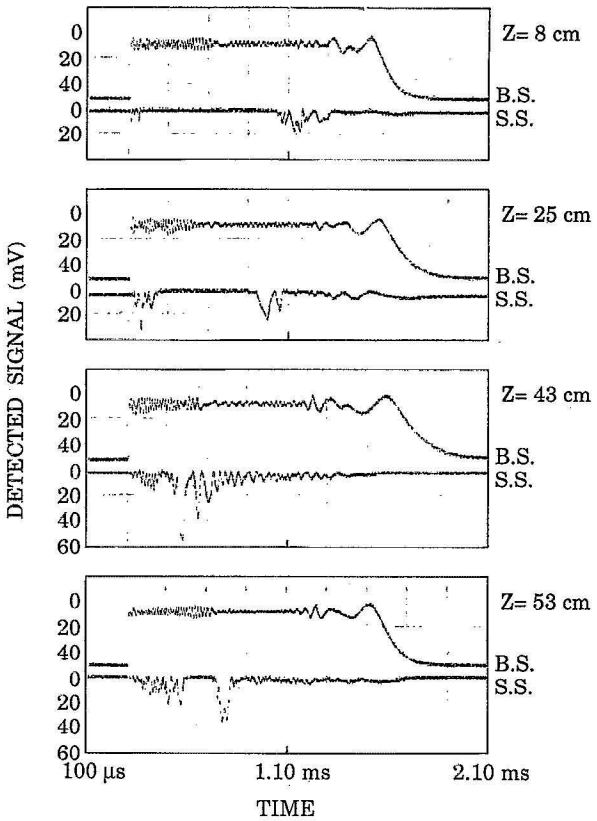

FIG. 15. Time evolution of backscattered signals (upper traces) and sidescattered signals (lower traces) at different locations z; polarization of incident signal in y direction and of scattered signal in z direction. Frequency is 10 GHz, charging potential is 8.5 kV, pressure is 72 mTorr, and reflection baseline (flash plate without plasma) is 7.5 W.

their separation diminishes with z is common among these figures and Fig. 12. The power levels, however, are significantly lower, when the setting of attenuators is taken into account. In a comparison of the peak power levels made at 13.77 GHz for scattering in the x-x orientation versus the x-z orientation, the former was higher by a factor of ≈ 10 dB in the general vicinity of the flash plate. The ratio decreased at greater distance from the flash plate.

Also included in Figs. 12, 14, and 15 are simultaneous traces of the backscattered signal, (denoted by B.S. in the margin of the graphs, while the sidescattered signal is denoted by S.S.). Here the bridge was not fully balanced, so that the backscattered signal also includes phase-shift information.

VI. TIME EVOLUTION OF TRANSVERSE TRANSMISSION

Measurement of the transverse transmission of microwaves across the plasma at various locations and time periods provides a means of studying the time history of the regions of supercritical density in the plasma. These observations were taken by using a radially located horn as the sending horn with another one located opposite to it for receiving the signal (see Fig. 1). The axial location of the two horns could be varied. When the transmission is almost completely cut off, a region of supercritical density can be assumed between the horns.

Figure 16 shows the time evolution of transverse transmission at various locations for a charging potential of 3.5 kV, background pressure of 13 mTorr, and frequency of 10 GHz. At each location three observations of successive plasma shots were superimposed, so as to give an indication of shot-to-shot variations. The diagram also shows the wave form of a current pulse sent through the plasma guns, for comparison of duration. The general nature of the traces shows that near the flash plate the transverse transmission is cut off almost in synchronism with the rise of the discharge current. Transmission is blocked for nearly 300 μs which is nearly an order of magnitude longer than the full width at half-maximum (FWHM) duration of the current discharge (even for this relatively low value of charging potential). At greater distances from the flash plate the duration of the cutoff in the transverse transmission is reduced. Furthermore, there is an intermediate period of reduced transmission whose duration increases with distance z. After the period of complete transmission cutoff, the transmission slowly increases.

Figures 17(a) and 17(b) show the time evolution of transverse transmission for three different charging potentials for a background pressure of 13 and 45 mTorr, respectively. The duration of complete transmission cutoff

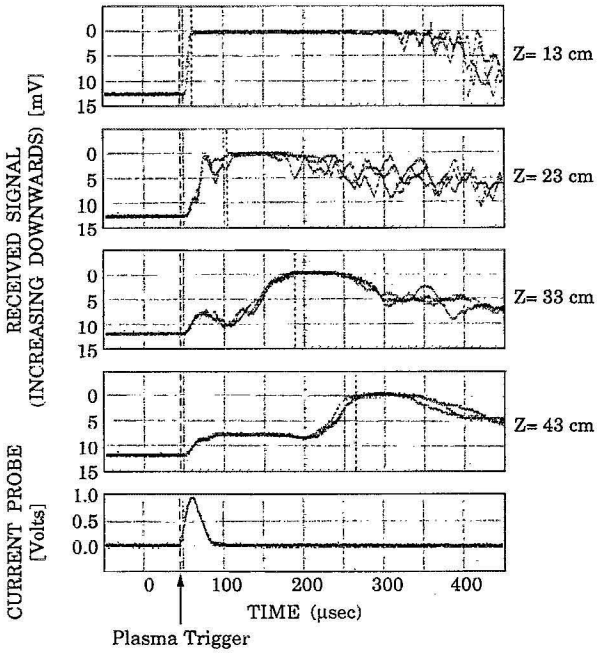

FIG. 16. Time evolution of transverse transmission at various distances z from the flash plate; frequency is 10 GHz, pressure is 13 mTorr, and charging potential is 3.5 kV. Three shots superimposed for each value of z.

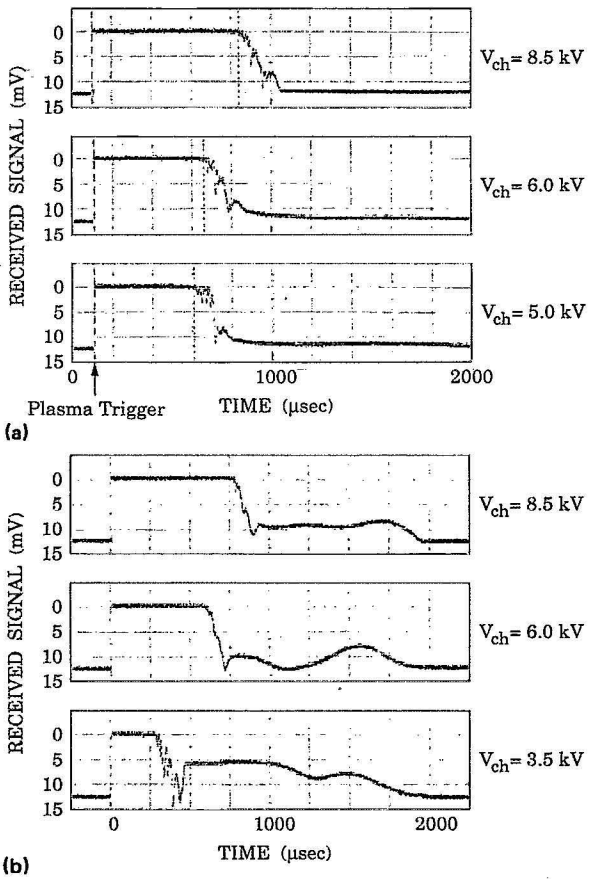

FIG. 17. (a) Time evolution of transverse transmission near flash plate (z=8 cm), for different charging potentials V_{ch}; frequency is 10 GHz, pressure is 13 mTorr. (b) Time evolution of transverse transmission near flash plate (z=8 cm), for different charging potentials V_{ch}; frequency is 10 GHz, pressure is 45 mTorr.

diminishes as the charging potential is reduced. This cutoff period is followed by a period of rapid fluctuations. The received signal rises to almost the full value that existed prior to firing the plasma guns for the case of 13 mTorr pressure. However, for 45 mTorr pressure the signal falls again and reaches a plateau followed by some further undulations, until the original level is restored.

VII. THE CRITICAL DENSITY BOUNDARY AND ITS CORRELATION WITH SIDESCATTERED SIGNALS

Based on the observations made of transverse transmission, plots have been made of the position of the critical density plasma layer as a function of time. Two such curves for the case of charging potentials 8.5 and 3.5 kV are shown in Fig. 18. As may be expected, the boundary for the latter lies inside the former, the duration of the supercritical boundary being shorter in the latter case. Another noteworthy feature is the plumelike shape appearing at large values of z.

Measurements of the position of the peak sidescattered signal (horns in the orientations x and x) as a function of time have also been made, and are shown along with the critical density boundary in Figs. 19(a) and 19(b) for the cases of charging potential 8.5 and 6 kV, respectively. As can be readily seen, the sidescattered signal appears to originate at or near the critical density layer.

An experiment to test the correlation of the sidescattered microwaves with the position of the critical density layer was also conducted at 13.77 GHz. Results are plotted in Fig. 20. For these measurements the charging potential was 8.5 kV, and the orientation of the horns corresponded to x-x polarization. It is seen that the duration of supercritical plasma density is less than for the 10 GHz studies. This is as expected since the critical plasma density is

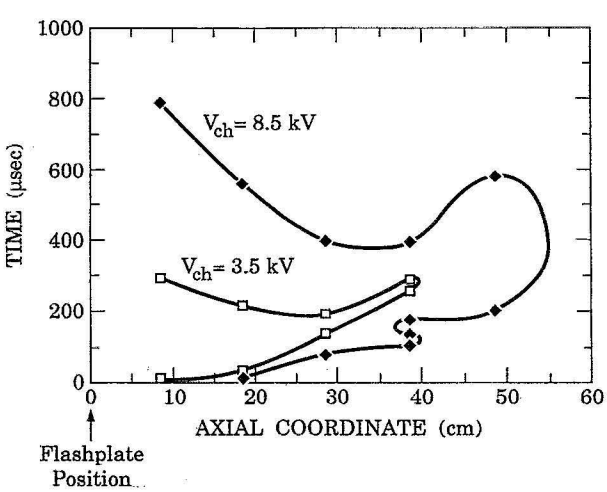

FIG. 18. Time evolution of critical density boundary as a function of location for charging potentials of 8.5 and 3.5 kV; frequency is 10 GHz, background pressure is 45 mTorr, and microwave power ≅30 mW.

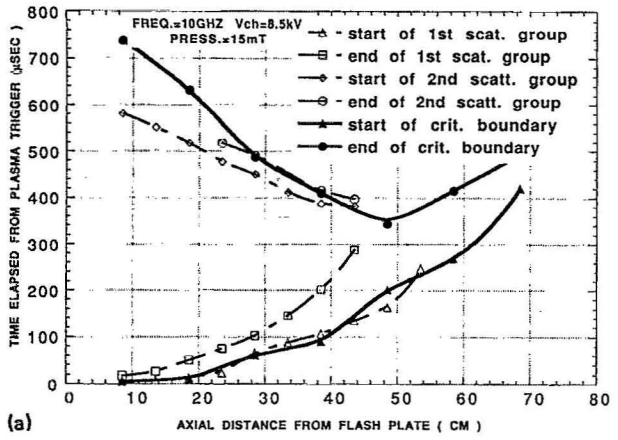

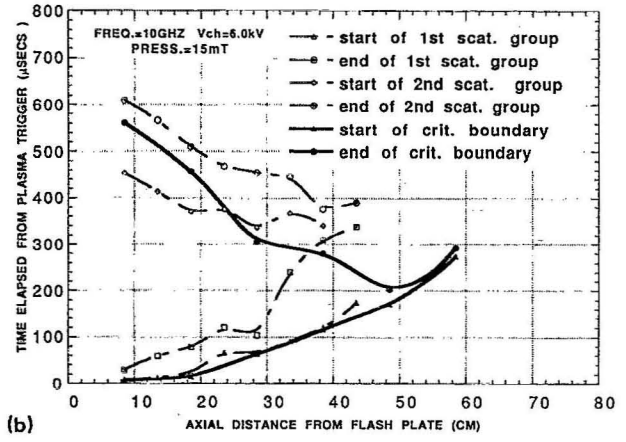

FIG. 19. (a) Correlation of sidescattered signal with critical density boundary; frequency is 10 GHz, pressure is 15 mTorr, incident microwave power level is 19 W, and charging potential is 8.5 kV. (b) Correlation of sidescattered signal with critical density boundary; frequency is 10 GHz, pressure is 15 mTorr, incident microwave power level is 19 W, and charging potential is 6 kV.

higher in this case. Once again, the sidescattered radiation appears to originate at or near the critical density layer.

VIII. AMPLITUDE OF THE SIDESCATTERED SIGNAL AND ITS 3D PLOT

Apart from correlations of the timing and location of the sidescattered radiation with those of the critical density layer, we have studied the amplitude of the scattered radiation. Figure 21 gives the variation of the peak of sidescattered signal with axial distance from the flash plate. The curves in the graph show the peak values averaged over eight shots for the two groups of sidescattered pulses when the plasma density is rising and falling, respectively. An interesting feature is the dip in the vicinity of 30 cm axial distance. It is attributable to attenuation of incident microwaves caused by a short-lived plume of a low-density plasma that proceeds ahead of the main body of the plasma as it propagates away from the flash plate. An indication of shot-to-shot variations can be had from the data points included in the diagram for single shots instead of the averaged eight shots.

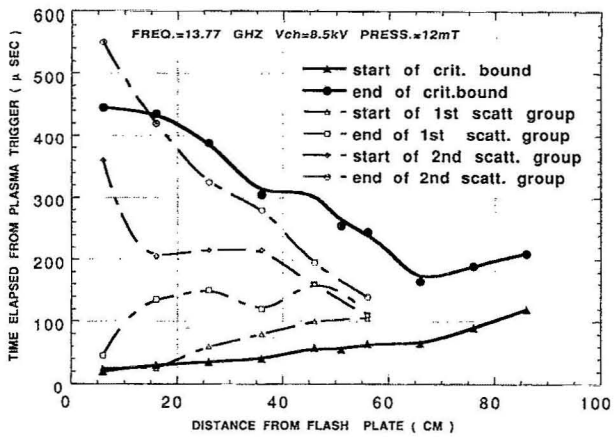

FIG. 20. Correlation of sidescattered signal with critical density boundary; frequency is 13.774 GHz, charging potential is 8.5 kV, and pressure is 12 mTorr.

In order to get an overview of the trends of amplitude variation, we approximated the envelope of each of the two sidescattered signal groups with the least-squares fit of a Gaussian curve. The coordinates interpolated from the Gaussian curves provide arrays of data for the two groups. These were then used to produce three-dimensional plots which give the shape of the envelopes as a function of time and axial distance. In this process the details regarding individual pulses or fluctuations that ride on the envelope are smoothed out. Hence the 3D plot represents general trends and not the fine structure. The 3D plot shows the peaks at 11 discrete values of axial coordinate, which makes them stand out in an isolated fashion. A dotted line has been added to the plot to indicate a continuous ridge, as a closer approximation. Figure 22 shows such a plot. The two ridges are far apart near the flash plate and tend to merge into one ridge farther away. They are reminiscent of the two-dimensional graphs in Figs. 19(a) and 19(b) even though the precise layout in time and axial coordinate is somewhat different.

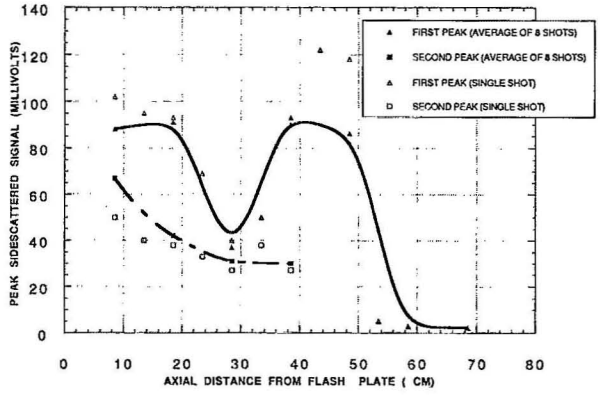

FIG. 21. Time evolution of peak sidescattered signal averaged over eight shots, at various axial distances from flash plate. Some data points from single shots are also shown for comparison.

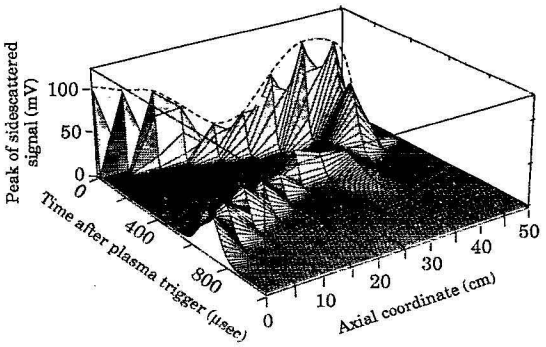

FIG. 22. Three-dimensional plot of the envelope of sidescattered radiation with respect to time and axial distance coordinates. The pulses and fluctuations in the scattered signal are smoothed by a Gaussian approximation of the envelope of the sidescatter signal.

IX. ESTIMATION OF PERCENTAGE OF SIDESCATTERED SIGNAL

In order to estimate the fraction of the incident power that is sidescattered, it is necessary to integrate the measured power density over the entire circumference of the plasma tube as well as over an axial length greater than that of a horn at a single position. In addition, contributions can also come from different polarizations. The orientations of the transmitting horn and the horn that receives the sidescattered signal can be adjusted in four different combinations. They represent the two orientations of the incident E field, namely along x and y axes in combination with the orientations of the received E field, namely along x and z axes, according to the direction of the three axes shown in Fig. 1. Rotation of the receiving horn provides data on the two possible planes of polarization of the scattered signals. Rotation of the plane of polarization of the incident microwaves provides information on the variation of the scattered radiation with polar angle. This last variation provides two values for the scattered signal equivalent to putting the receiving horn at azimuthal angles, $\phi=0°$ and $\phi=90°$. Furthermore, it is necessary to estimate the values obtained for other azimuthal positions. Making use of system symmetries and because diffusion and recombination in plasma can be considered as smoothly varying processes, we assume that the variation of scattered power with ϕ goes as

$$p(\phi)=c_1+c_2\sin^2\phi,$$

where $c_1=P_{\min}$, $c_2=(P_{\max}-P_{\min})$, and $P_{\max}$ and $P_{\min}$ are the measured scattered power for the two azimuthal positions. It was observed that $P_{\min}$ was $\approx 0.65P_{\max}$ near the flash plate, while the ratio of $P_{\min}$ to $P_{\max}$ became nearer to unity near the opposite end of the tube. This could be attributed to the homogenizing effect of stray reflections within the tube.

The following simplifying assumptions were made regarding the receiving horn: (a) the power density of radiation is uniform across the aperture of the horn; (b) the effective area of the horn for purposes of determination of directivity is $(8/\pi^2)AB$, where A is the length and B the width of the mouth of the horn[11]; (c) most of the power enters within the main lobe of the radiation pattern of the horn.

The power received over a strip around the plasma tube whose length is the same as the dimension of the horn that is parallel to the axis is obtained by integrating $p(\phi)$ over the azimuthal range. In the case where the horn is oriented to receive E_x,

$$p_{\text{strip}}=(2\pi r/B)(c_1+0.5c_2),$$

where r is the radius at which the receiving horn is located. The denominator is replaced by A when the receiving horn is oriented to receive E_z. A summation of p_{strip} for strips down the length of the tube provides an estimate of the total scattered power flux at a given instant of time. The process can be repeated at numerous other instants of time and the scattered energy over a given interval of time can thus be evaluated. This result was compared initially with the energy reflected when no plasma was present.

A time interval of 80 μs was chosen for the integration of the sidescattered power producing the energy estimate. In this period practically all the scattered energy is in the vicinity of the flash plate. For the case where E_z is the received polarization, this time interval is covered by three axial positions of the receiving horn at 4.5, 12.5, and 21.0 cm from the flash plate. At each position eight shots of the pulsed plasma were used to determine an average so as to minimize the effects of shot-to-shot jitter. The E field of the incident signal was in the y direction. The ratio of the measured scattered energy to the energy reflected without the presence of plasma was evaluated as described earlier, and is calculated to be 5%.

In the case of E_x polarization for the scattered signal, the receiving horn has its large dimension A in the axial direction. Thus nearly the same axial length is covered in two positions of the horn. Fewer shots were taken in this case. The contribution of scattering is of the same order. This indicates that the ratio of the scattered energy to the reflected energy without plasma is about 10% including both polarizations, E_z and E_x, of the scattered signal. It is estimated that with no plasma the reflected energy received at the transmitting horn is about 10% lower than energy incident on the flash plate. The ratio of scattered energy to the energy incident on the flash plate is correspondingly reduced to an estimated value of 9% from the above measurements.

Using the same basic techniques without integration with respect to time, we evaluated the ratio of the peak value of instantaneous scattered power to that of reflected power without plasma. These peak ratios are shown in Table I, for various parameters regarding charging potential, polarization of incident and scattered waves, and background pressure. A trend that is noticeable is that the ratio of peak scattered power to incident power increases as the pressure of the background gas is increased. The instantaneous peak power levels for different parameters and polarizations cannot be added directly as the exact timing of the peaks may not be the same. These figures are presented here so as to provide an estimate of percentages

TABLE I. Ratio of peak scattered power to incident microwave power, for different values of charging potential, polarization, and pressure of background gas.

V_{charge} (kV)	Polarization		Pressure of background gas (mTorr)	Ratio of peak scattered power/ incident power
	Incident	Scattered		
8.5	E_y	E_z	75	17%
8.5	E_x	E_z	75	15%
8.5	E_x	E_x	52	13%
6.0	E_y	E_z	72	22%
6.0	E_x	E_x	56	13%
6.0	E_x	E_x	15	10%
3.5	E_x	E_x	56	10%
3.5	E_x	E_x	15	5%

even at the peak levels of scattered signal. Since this scattered signal accounts at best for no more than about one-fourth of the incident signal, it is clear that other mechanisms are responsible for the bulk of the reduction in the backscattered signal.

X. ESTIMATION OF REDUCTION IN BACKSCATTER FROM COLLISIONAL EFFECTS IN A TRANSVERSELY HOMOGENEOUS PLASMA

Collisional effects would play a minimal role when the background pressure is low, as in our high-power experiments,[9] where it was 0.1 mTorr. However, the same cannot be said for higher pressures, as was the case in the present experiments. A study of the reduction in backscatter due to collisional effects was made for the parameter range of interest here. The approached used is that employed by Vidmar in Ref. 1, and briefly outlined here. The plasma density is assumed to be homogeneous in the transverse direction and to have an Epstein profile in the axial direction, given by the relation

$$n=n_0/[1+\exp(-z/\sigma)],$$

where σ represents the rate of variation of plasma density n, which goes from 0 to n_0 as z goes from $-\infty$ to ∞. Microwaves propagating up the density gradient get partially reflected. The component that is partially transmitted proceeds toward the conducting plate and gets reflected. The absorption is evaluated by integrating the imaginary part of the propagation constant in the collisional plasma over the forward as well as backward path. This returning signal is added to that reflected from the plasma profile. Subject to the approximations made in modeling the plasma, the approach gives the estimated total reduction in backscatter caused by the presence of this plasma. The values are a function of the gradient scale factor of the density profile, the momentum-transfer collision frequency, the angle of incidence, and the relative values of the frequency of incident microwaves and the maximum plasma frequency. Using the above approach and assuming a gradient scale factor of 10 cm, a maximum plasma frequency of 10 GHz, and normal incidence of microwaves of 10 GHz frequency, the peak reduction in backscatter varies from 2 to 25 dB as the momentum-transfer collision frequency varies from 2×10^7 to 2×10^8 s^{-1}. An increase in the angle of incidence makes for a reduction in the peak attenuation occurring at resonance between the two frequencies.

The momentum-transfer collision frequency is a function of the gas composition, the pressure, and the electron temperature. This last had been earlier estimated[9] to be $\approx$2 eV, based on Langmuir probe measurements. Taking the case of dry air and a typical pressure of 15 and 75 mTorr in the low-power experiments, and using curves in Fig. 7 of Ref. 12, the momentum-transfer collision frequency is estimated as 5×10^6 and 2.5×10^7 s^{-1}, respectively. This indicates that based on this model the contributions to reduction in backscatter due to collisional effects would be rather small for parameters relevant to these experiments.

In fact, in the experiments an increase of the background pressure produced a decrease in the maximum attenuation in the case of 3.5 kV as charging potential (Fig. 8), but did not alter it significantly from the maximum observable attenuation for the case of 8.5 kV charging potential. The greater sensitivity of the observation in the former case gives a clue as to the nature of the underlying physical phenomena. With increases in background pressure the collision frequency between the electrons and neutrals would tend to increase. As discussed above, an increase of the collision frequency would by itself tend to increase the maximum attenuation. Consequently, it is clear that additional mechanisms must be responsible for the attenuation besides collisions between electrons and neutrals.

XI. SOME FEATURES OF THE PHYSICAL PHENOMENA UNDERLYING THE GENERATION OF THE PLASMA

The four plasma guns are discrete sources of plasma generation whose lateral dimensions are small ($\approx$0.5 cm) compared with the tube diameter ($\approx$30 cm). The flow of discharge current through the inner conductor generates a magnetic field that surrounds the conductor. Thus the charged particles in the arc would have axial Lorentz forces exerted on them by the magnetic field.[13] These are seen to be directed away from the opening in the coaxial conductors that generate the arc. Because of their lighter mass, the electrons would achieve higher velocities than ions. They would thus streak out of the ports of the plasma guns, causing ionization by collision with molecules of the residual gas in their path. The plasma so generated is likely to be inhomogeneous in the transverse direction. This means that the layer of critical density would not be a plane surface. The curvature and ripples in it would cause the local incident angle to be nonzero, even when the overall geometry of the experiment implies normal incidence. This in turn influences absorption as well as sidescatter.

The observations on the time and location of the critical density layer (determined from transverse transmission data) (Figs. 18–20) indicate that a plume of the plasma proceeds rapidly away from the flash plate and

begins to decay. It is followed by another component of the plasma which moves and decays more slowly than the plume. The charged particles causing the plume could thus be the above-mentioned streams of fast electrons shot out from the plasma guns by Lorentz forces acting on the discharge current. In its path the plume would generate ionization by collision, and create less-energetic electrons and ions which constitute the more slowly moving and slowly decaying component of the plasma.

The data on transverse transmission taken at a low value of charging potential (3.5 kV) lend further support to the above viewpoint. It is seen from the trace for $z=43$ cm in Fig. 16, that there is a plateau in the reduction of received signal starting just after the end of the discharge current and lasting for about 100 μm. In this period the transmission is not fully blocked, but is attenuated. It is followed by a period in which the attenuation rises to near total blockage. In other words, at somewhat distant points from the flash plates there exists a precursor to the main body of the plasma. It blocks the transverse transmission only partially presumably because of subcritical density, or incomplete filling of the plasma tube in the radial direction at that distance.

The timing of the observed sidescattered microwave signals correlates closely with the transitions of the critical density layer past the receiving horns (Figs. 19 and 20). This shows that the sidescattered signal originates at or near the layer of critical density.

XII. RESONANCE ABSORPTION IN A TRANSVERSELY INHOMOGENEOUS PLASMA

Considering that the plasma is generated by four plasma guns, it is likely that the layer of critical density will have ripples and turbulence as discussed above. Recombination of plasma at the walls would also tend to give radial variations of plasma density, resulting in a curved geometry for the layer of critical density. Accordingly, the angle of incidence of microwaves on the layer of critical density would be nonzero at most places, unlike what could be anticipated from a simple model of the experiment. An additional source of instability in the plasma resulting in transverse inhomogeneity can arise from a non-Maxwellian distribution of energy of electrons. The resulting "free energy" can be transferred to fluctuating fields.[14]

It is relevant to examine the phenomenon of "resonance absorption" occurring when electromagnetic radiation propagates up the density gradient in a plasma at a finite incident angle with respect to a layer of critical density. When θ is nonzero, an electromagnetic wave, which has its electric vector lying in the plane of incidence (p polarization), has a finite component of E field parallel to the density gradient. This results in electron oscillations which build up resonantly near the critical density, and cause a density fluctuation. This appears as electron plasma waves which contribute to enhanced scattering[15] as well as resonance absorption.[16,17] It may also be noted that this effect has a broad maximum at a value of θ lying between 0° and 90°. It is small near $\theta=0$ as the E-field component parallel to the gradient tends to vanish. It is also small at values of θ approaching 90° as the electromagnetic wave gets reflected at a layer well ahead of the critical density; so that the evanescent E field reaching the resonance layer is very small. The peak resonance absorption is of the order of 0.5,[18] for the optimum incident angle for a laterally homogeneous layer of critical density.

The effect of ripples on the layer of critical density has been studied by Rowland using numerical as well as analytical techniques.[19] The ripples enhance the absorption. A parameter $k_f L/k_t a$ has been defined in which L is the density gradient scale factor, k_t is the propagation factor for the ripples on the layer of critical density, and a is the amplitude of the same. In a simplified model the absorption scales as $\exp(-k_f L/k_t a)$. Simulations show cases of up to 90% absorption of incident energy.

As a consequence of the preceding analyses, it is believed that a major part in the reduction of backscatter is caused by the lateral inhomogeneity in the plasma and by the process of resonance absorption. Sidescatter and collisional absorption play lesser roles. The relative values would be dependent on the array of input parameters. The absorption can thus be explained without invoking nonlinearities caused by the power level of incident microwaves. This agrees with experimental observations.

XIII. CONCLUSIONS

Backscatter, sidescatter, transverse transmission, and axial transmission of low-power microwaves interacting with a pulsed plasma have been studied experimentally over a range of parameters. Measurements of the time evolution of the position of the critical density layer indicate that a plume propagates rapidly away from the flash plate and is followed by a more slowly moving plasma front of higher density. This plume decays more rapidly than the main body of the plasma. A possible cause of the observed phenomena is the presence of more than one plasma species emanating from the plasma guns.

A reduction in backscatter was obtainable down to the limits of our observational accuracy ($\approx$30 dB attenuation). The timing of the observed sidescattered microwave signals correlates closely with the transitions of the critical density layer past the receiving horns. It is therefore evident that the sidescattered signal originates at or near the critical density layer. The sidescattered signal is linearly dependent upon the incident power over three orders of magnitude.

The processes of resonance absorption and sidescatter at the layer of critical density can account for a large part of the observed reduction in backscattered signal. Attenuation due to collisional effects between electrons and neutrals is not significant at pressures below 10 mTorr, but can play a role at higher pressures.

ACKNOWLEDGMENTS

Discussions with Professor H. Fleischmann, Dr. R. J. Vidmar, Dr. H. L. Rowland, and Dr. W. Main were very

useful. Valuable help was rendered by Jay Pyle in the setting-up phase of the experiment. The work is supported by AFOSR.

[1] R. J. Vidmar, IEEE Trans. Plasma Sci. **PS-18**, 733 (1990).
[2] R. J. Vidmar, in International Conference on Plasma Science, Williamsburg, VA, June 3–5, 1991, p. 86.
[3] D. T. Moriarty, K. D. Vilece, M. Onozuka, R. F. Duraski, C. Yoo, and M. C. Lee, in International Conference on Plasma Science, Williamsburg, VA, June 3–5, 1991, p. 146.
[4] M. Laroussi and J. R. Roth, in International Conference on Plasma Science, Williamsburg, VA, June 3–5, 1991, p. 146.
[5] D. Gregoire and J. Santoru, in International Conference on Plasma Science, Williamsburg, VA, June 3–5, 1991, p. 86.
[6] J. E. Sharer, O. C. Eldridge, S. F. Chang, M. H. Bettenhaussen, and N. T. Lam, in International Conference on Plasma Science, Williamsburg, VA, June 3–5, 1991, p. 87.
[7] A. Y. Ho and S. P. Kuo, in International Conference on Plasma Science, Williamsburg, VA, June 3–5, 1991, p. 89.
[8] W. W. Destler, P. Catravas, J. Rodgers, A. Singh, C. D. Striffler, P. E. Latham, and H. L. Rappaport, in International Conference on Plasma Science, Williamsburg, VA, June 3–5, 1991, p. 147.
[9] W. W. Destler, J. E. Degrange, H. H. Fleischmann, J. Rodgers, and Z. Segalov, J. Appl. Phys. **69**, 6313 (1991).
[10] I. Alexeff, F. Dyer, and M. Rader, in International Conference on Plasma Science, Williamsburg, VA, June 3–5, 1991, p. 86.
[11] S. Ramo, J. R. Whinnery, and T. van Duzer, *Fields and Waves in Communication Electronics* (Wiley, New York, 1984), p. 618.
[12] R. D. Hake, Jr. and A. V. Phelps, Phys. Rev. **158**, 70 (1967).
[13] R. A. Gross and B. Miller, *Methods of Experimental Physics* (Academic, New York, 1970), Vol. 9, Part A, Sec. 5.13.
[14] W. A. Perkins, *Methods of Experimental Physics* (Academic, New York, 1970) Vol. 9, Part A, Sec. 7.3.
[15] J. Sheffield, *Plasma Scattering of Electromagnetic Radiation* (Academic, New York, 1975), Chap. 10.
[16] A. V. Gurevich, *Nonlinear Phenomena in the Ionosphere*, translated by J. G. Adashko (Springer, Berlin, 1978), Sec. 6.2.
[17] Z. Sedlacek and B. Roberts, J. Plasma Phys. **41**, 97 (1989).
[18] W. L. Kruer, *The Physics of Laser Plasma Interactions* (Addison-Wesley, Reading, MA, 1988), Sec. 4.2.
[19] H. L. Rowland (unpublished).